Improvement of the Shift Bump Magnetic Field for a Closed Bump Orbit of the 3-GeV RCS in J-PARC

T. Takayanagi, K. Kanazawa, T. Ueno, H. Someya, H. Harada, Y. Irie, M. Kinsho, Y. Yamazaki, M. Yoshimoto, J. Kamiya, M. Watanabe, M. Kuramochi, and K. Satou

***Abstract*—The four shift bump magnets (BUHS01-04) of the 3-GeV RCS in J-PARC, which are located at the long straight section, produce a fixed main bump orbit to merge the injection beam into the circulating beam. They are realized with four magnets connected in series to form the accurate closed bump orbit. However, the total integrated magnetic field of the four magnets is not zero because of the magnetic field interference between the shift bump magnet and the adjacent quadrupole magnets (Q magnet). In order to measure the magnetic field distribution accurately, the short search coil and the long search coil were used. Furthermore, the imbalance of the total integrated magnetic field has been improvement by inserting 0.3 mm insulators in the median plane of the return yoke of the BUHS02 and 03. The value of the integration has been decreased from 2358.0 G · cm to −71.6 G · cm.**

***Index Terms*—Bump magnet, interference of the magnet, magnetic field measurement, 3-GeV RCS in J-PARC.**

I. Introduction

J-PARC (Japan Proton Accelerator Research Complex) accelerator consists of three accelerators, a linear accelerator (Linac), a rapid cycling synchrotron (3-GeV RCS) and a main ring (50-GeV MR). The beam injection system of the 3-GeV RCS is composed of four shift bump magnets, four horizontal paint bump magnets and two vertical paint magnets.

The four shift bump magnets, which make the injection bump orbit, are placed in line at the beam injection area of the 3-GeV RCS [1]–[3]. Furthermore, the Q magnets (QFL and QDL) are placed next to each shift bump magnet (BUHS01 and 04) respectively, as shown in Fig. 1.

The integrated magnetic field of each shift bump magnet is decreased because of the interference with each magnet, and the degree of the decrease is varied with the various spatial conditions. Accordingly, it is necessary to adjust the imbalance so that the total integrated magnetic field of four shift bump magnets may be zero.

The accurate data on the magnetic field distribution in the injection area is necessary for modeling the beam injection system of the 3-GeV RCS. In order to measure the magnetic field distribution in situ, the shift bump magnet and the Q magnet were made arrangement of an actual combination in the laboratory. Furthermore, the magnetic field distribution after installation in the injection area of the 3-GeV RCS was also measured to take into account the influence of the vacuum chamber, and the results were compared.

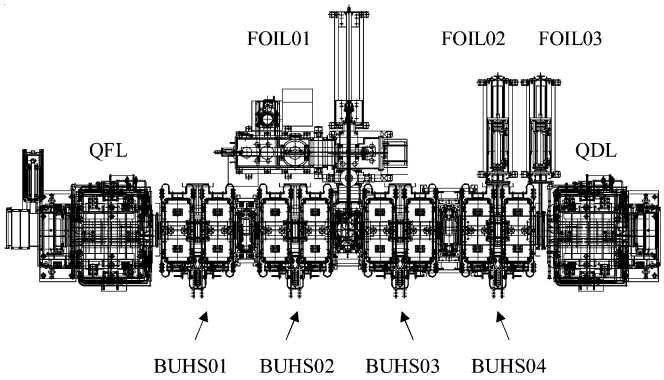

Fig. 1. Schematic view of the injection area. Four shift bump magnets (BUHS01-04) and two Q magnets (QFL and QDL) are arranged.

II. Magnetic Field Measurement

A. Mapping Bar of the Short Search Coil

To measure the magnetic field distribution in a wide area, the mapping bar where 124 short search coils is aligned in line at intervals of 20 mm was produced. The short search coil is 10 turns and its wound by 0.1 mm enameled wire. The bobbin of the short search coil is made of Bakelite and the diameter is 5.98 mm. The mapping bar made of FRP is having H structure, which is 40 mm in width and 60 mm in height and the length is 3000 mm. The mapping bar is fixed at the both ends to the moving stage of two axes. Near the center of the mapping bar was sagged 0.1 mm by its weight. However, the difference of the perpendicular component By that is compared at the central position and the end position was less than 0.01%. So the influence of the sag of the mapping bar is negligible.

The mapping bar is extended by 1500 mm when the interference between the two magnets is measured. In that case, the support stand for the mapping bar is placed on the iron core of the shift bump magnet, and the sag to be less than 0.1 mm. So the influence of the sag by the extension is negligible.

The actual combination was achieved by combining two magnets, for example the QFL and the BUHS01, and the magnetic field distribution of the shift bump magnet that influenced by the interference was measured. The picture of the shift bump magnet, the mapping bar and the support stand are shown in Fig. 2.

B. Calibration of the Short Search Coil

The diameter of all the bobbins was measured by the digital slide calipers with the accuracy of 1/100 mm, and only those

Manuscript received August 30, 2007.

T. Takayanagi, K. Kanazawa, T. Ueno, Y. Irie, M. Kinsho, Y. Yamazaki, M. Yoshimoto, J. Kamiya, M. Watanabe, M. Kuramochi, and K. Sato are with the JAEA J-PARC, 2-4, Shirakata, Shirane, Tokai-Mura, Naka-Gun, Ibaraki-Ken, 319-1195, Japan (e-mail: takayanagi.tomohiro@jaea.go.jp).

H. Someya is with the KEK, Tsukuba-shi, Ibaraki-Ken, 305-0801, Japan.

H. Harada is with the Hiroshima University, 1-3-1 kagamiyama, Higashi-Hiroshima, Hiroshima, 739-8526, Japan.

Digital Object Identifier 10.1109/TASC.2008.920768

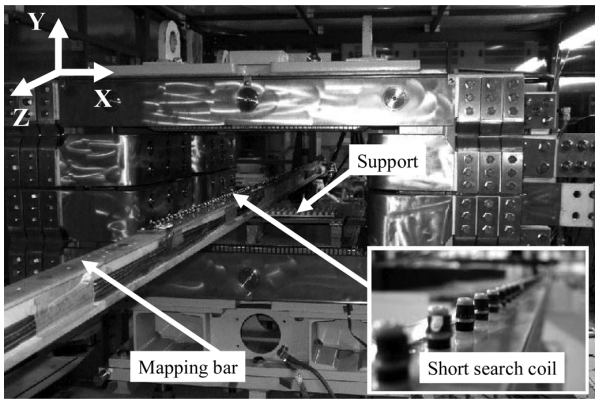

Fig. 2. Picture of the shift bump magnet in the laboratory. The mapping bar with 124 short search coils and the support stand which prevents sag of the bar.

with 5.98 mm diameter were chosen. However, since the enameled wire was wound manually, the individual difference of the effective area was arisen. Therefore, each coil of 124 pieces was calibrated by the calibration magnet.

The calibration magnet is a permanent magnet that central magnetic field is 386 mT. The short search coil is fixed to the turntable that spins at 1 Hz, and the output voltage of the short search coil is measured by using an FFT analyzer. The turntable and a magnetic probe (NMR) are placed 50 mm apart to avoid a collision each other. Therefore, the coefficient k (0.9995) was computed by the magnetic field at the position of the short search coil from the position of the magnetic probe.

The output voltage (V) for the calibration area of the short search coil (S) was determined by the average of three measurements. As a result, there was the difference of 1.0% or less among of the 124 pieces. However, each short search coil that the calibration has been done is used for the measurement, and so the difference is negligible. The equation of the computing the calibration area of the short search coil, as in

$$S = V \cdot N/(\omega \cdot B \cdot k) \tag{1}$$
$$\times \begin{cases} V : Voltage\,(FFT) \\ N : Volume\,(10Turn) \\ \omega : 2\pi\pi\ (Hz)\ Angular\ frequency \\ B : Magnetic\ flux\ density\,(NMR) \\ k : Calibration\ factor\ of\ the\ NMR\ and\ coil. \end{cases}$$

C. Analysis Method of Signal Processing

The output voltage of each short search coil was measured by WE7000 [4]. The number of input terminals of the WE7000 is ten and the signals of them are measured simultaneously. In order to measure the voltage of 124 short search coils, two rotary switches were used. The rotary switch has four channels moved simultaneously and sixteen terminals at each channel. The two rotary switches were turned at 16 rotations at the same time, and the voltage of all short search coils was measured. Moreover, there is 0.5% fluctuation of the exciting current of the power supply every pulse shot, and so the search coil voltage was normalized by the exciting current measured simultaneously with each search coil voltage.

The input channels of the WE7000 have each offset voltage (dV). To remove the offset voltage, the changeover switch was used. The signal of the short search coil of the same condition was measured twice by changing a signal polarity with the changeover switch. By adding each measurement result, the offset voltage is eliminated. The schematic view of the measuring the short search coil voltage and the date processing are shown in Figs. 3 and 4(a), respectively.

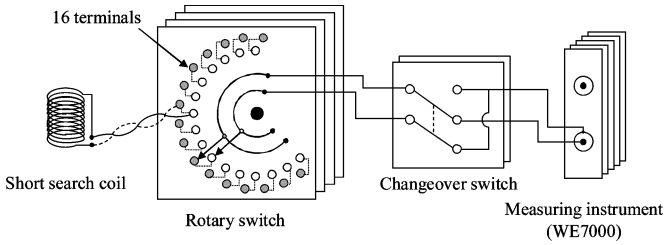

Fig. 3. Schematic view for measuring the short search coil voltage.

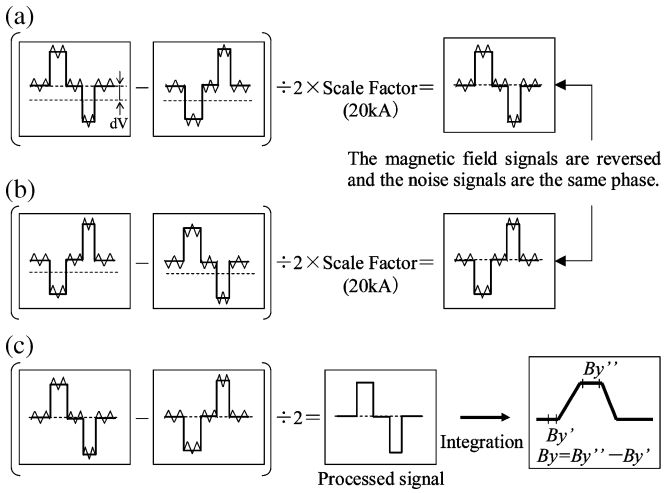

Fig. 4. Offset and noise eliminations for magnetic field data. (a) Removal of the offset (dV) of the measuring instrument by the changeover switch; (b) coil reversal and changeover switch; (c) calculation By.

The signal from the search coil has the noise by the pulse magnet. In order to remove the noise, the mapping bar was reversed in the same position. In this case, although the true signal of the magnetic field is reversed, the noise signal is remained in the same phase, as shown in Fig. 4(b). The true signal can be obtained by subtracting the signal in Fig. 4(b) from that in Fig. 4(a). The voltage thus obtained is integrated, and the magnetic field (By) is computed, as shown in Fig. 4(c).

III. Measurement Results of the Magnetic Filed

A. Result of the Calibration

The comparison with before and after calibration was performed using the measurement result of the BUHS01, as shown in Fig. 5. The offset voltage of the measuring instrument and the noise by the pulse magnet in each channel was eliminated. The magnetic field distribution has been measured accurately.

B. Characteristic of the Shift Bump Magnet

The relative difference of the integrated magnetic field distribution among of the four shift bump magnets was measured using the long search coil. The long search coil that is three turns with an enameled wire of 0.1 mm is 6 mm in width and 2500 mm in length. The measurement result of the integrated magnetic field distribution of the BUHS01 is shown in Fig. 6. The distribution is based on the center of the gap, and the ratio is

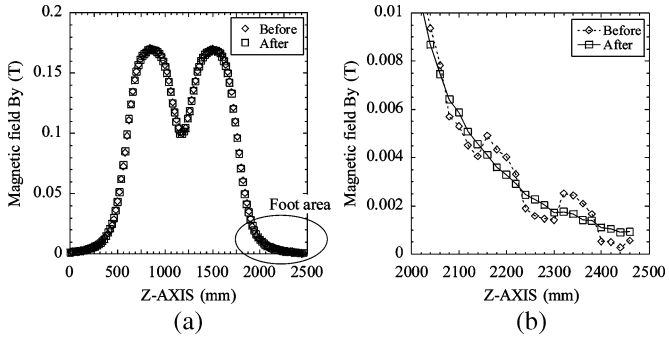

Fig. 5. Comparisons of the magnetic field distribution before and after calibrating: (a) distribution of the complete magnet and (b) details of the foot are.

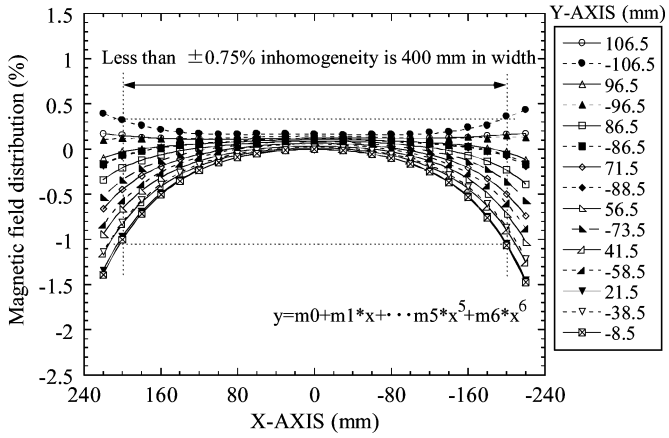

Fig. 6. Measurement result of the integrated magnetic field distribution of the BUHS01.

computed with $(BL_x - BL_0)/BL_0 * 100$. BL_x is the integrated magnetic field at each measurement position (x-axis), and BL_0 is the integrated magnetic field based on the center of the gap ($\mathrm{x} = 0, \mathrm{y} = 0$). The uniform field region with less than $\pm 0.75\%$ inhomogeneity is 400 mm in width. This result satisfies the acceptance for 486 $\pi\mathrm{mm} - \mathrm{mrad}$ beams that is equivalent to 370 mm in width and 240 mm in height.

The integrated magnetic field distributions of each shift bump magnet were compared, as shown in Fig. 7. The good agreement was obtained within a range of 0.05%. Furthermore, the difference of the integrated magnetic field at the center position of the magnetic field was less than 0.1%, as shown in Table I. It has been confirmed that there is no individual difference among of the four shift bump magnets. The difference is defined as the deviation from the averaged value over the four magnets.

C. Interference of the Magnetic Field

The measurement of the magnetic field variation by the interference with the adjacent magnets was performed by combining the two magnets in the laboratory. The interaction of the magnetic field and the influence of the iron core of the adjacent magnets are included in the interference.

Each measurement result was combined, as shown in Fig. 8. The distribution near the center of the iron core was in agreement with that for a single magnet distribution. However, the distribution of the foot area was decreased because of the interference. In additionally, since the spatial distance from the QFL (or QDL) to the next BUHS01 (or BUHS04) is different, the degree of the interference with two magnets is also different slightly. Each integrated magnetic field of the BUHS01

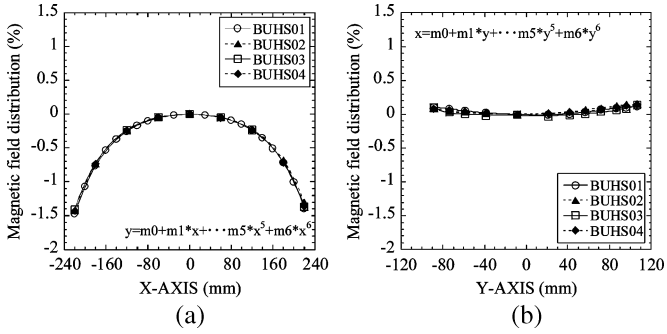

Fig. 7. Integrated magnetic field distributions of each shift bump magnet. (a) Distribution of the x-axis ($-220 < \mathrm{x} < 220, \mathrm{y} = 0$), (b) Distribution of the y-axis ($\mathrm{x} = 0, -90 < \mathrm{y} < 110$).

TABLE I
DIFFERENCE OF THE INTEGRATED MAGNETIC FIELD

BUHS01	BUHS02	BUHS03	BUHS04
-0.076 %	0.026 %	0.06 %	-0.01 %

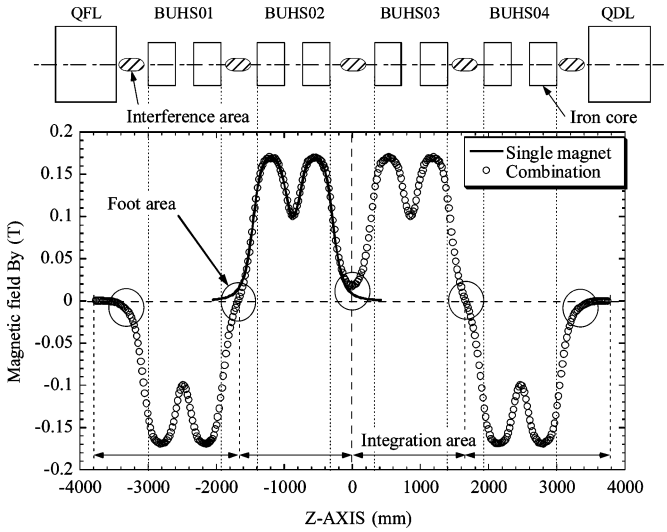

Fig. 8. Magnetic field measurement of the interference between the Q magnetic and the shift bump magnet and the suppression of each bump magnet.

and 04 was decreased by 0.67% and 0.57% as compared with the BUHS02 (or BUHS03), respectively. The imbalance of the total integrated magnetic field of the four shift bump magnets was increased. The integration area of the magnetic field is the point at the polarity change and the lowest point of the magnetic field (see in Fig. 8).

D. Adjustment of the Imbalance

The four shift bump magnets are connected in series, so the individual adjustment of the integrated magnetic field by the power supply is impossible. In order to improve the imbalance of the total integrated magnetic field, the method using the thin insulator made of a Rika-Light [5] has been examined. By inserting the insulators of 0.3 mm or 0.5 mm in thick to the median plane of each return yoke, the variation measurement of the integrated magnetic field was performed by using the BUHS01. The measurement and the calculation results are shown in Table II

TABLE II
DECREMENT OF THE INTEGRATED MAGNETIC FIELD

Insulator thickness	0.3 mm	0.5 mm
Measurements	-0.61 %	-0.87 %
Calculations	-0.20 %	-0.32 %

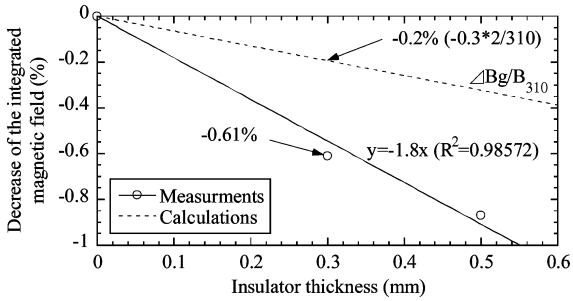

Fig. 9. Measurement result of the integrated magnetic field decrement by inserting the insulators. A solid line is the measurements and a dotted line is the calculations.

and Fig. 9, respectively. The equation of the calculation of the decrement, as in

$$B_y = \left(\mu_0 NI - \frac{B_{iron}L}{\mu_r}\right)\frac{1}{g} \tag{2}$$

$$\frac{\Delta B_y}{B} \approx \frac{\Delta g}{g} \tag{3}$$

$$\times \begin{cases} N = Ampere\ turn\ (AT) \\ B_{iron} = Magnetic\ field\ in\ the\ core\ (T) \\ B_y = Magnetic\ field\ in\ the\ gap\ (T) \\ L = Length\ of\ the\ magnetic\ field\ circuit\ (m) \\ \mu_r = Relative\ permeablity \\ g = Gap\ (m). \end{cases}$$

As a result, it has been confirmed that the integrated magnetic field can be adjusted by the method with insulators. By inserting the 0.3 mm insulators in the median plane of the return yoke of the BUHS02 and 03, the imbalance of the total integrated magnetic field was varied from $2358.0\ \mathrm{G\cdot cm}$ to $-71.6\ \mathrm{G\cdot cm}$ by using the experimental result. This decrement of the imbalance has been reduced the closed orbit distortion in the ring from 6.0 mm to less than 1.0 mm by the beam analysis soft of SAD.

Both of the reason of the difference between the measurement and the calculation and the experimental result of the distortion of the closed orbit will be reported at some other time.

E. Magnetic Field After Installation in the 3-GeV RCS

The measurement of the shift bump magnetic field after installation with no ceramic chamber in the 3-GeV RCS was performed. The short search coil of 10 mm in diameter that is twenty turns with an enameled wire of 0.1 mm was used.

The QFL and the QDL is installed with the ceramic vacuum chamber and both of the titanium chamber and the bellow are installed in the space between each shift bump magnet.

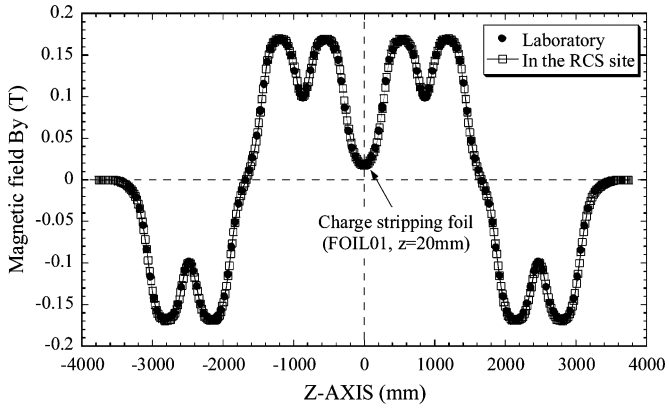

Fig. 10. Measurement result of the magnetic field distribution of four shift bump magnets that have been installed in injection area.

The measurement result is shown in Fig. 10. The distribution of the magnetic field after installation in the RCS site was agreed with the result of two magnets combination in the laboratory. Furthermore, this result was in agreement within 0.14% at the position of the charge stripping foil (see in Fig. 10) when the maximum value of the measurement result in the RCS site was normalized to that obtained in the laboratory. This difference can be disregarded as an error of the measurement because of the measurement in the locale cannot set up the coil in good accuracy.

IV. SUMMARY

The distributions of the magnetic field and the integrated magnetic field have been measured by both of the short search coil and the long search coil. Moreover, the measurement of the interference of the adjacent magnets was performed by combining the adjacent two magnets in situ.

By inserting 0.3 mm insulators in the median plane of the return yoke, the imbalance of the total integrated magnetic field of the four shift bump magnets has been improved.

The magnetic field distributions were measured both in the laboratory and in site at the RCS injection area, so they have been confirmed that these results are well in agreement.

ACKNOWLEDGMENT

The authors would like to thank all J-PARC members for the support. One of the authors (T. Takayanagi) is grateful to H. Harada for his calculation with the SAD.

REFERENCES

[1] T. Takayanagi *et al.*, "Design of the shift bump magnets for the beam injection of the 3-GeV RCS in J-PARC," *IEEE Trans. Applied Supercond.*, vol. 16, no. 2, pp. 1366–1369, Jun. 2006.
[2] T. Takayanagi *et al.*, "Design of the injection bump system of the 3-GeV RCS in J-PARC," *IEEE Trans. Applied Supercond.*, vol. 16, no. 2, pp. 1358–1361, Jun. 2006.
[3] T. Takayanagi *et al.,* in *Proc. 3rd Annu. Meeting Particle Accelerator Society of Japan and the 31st Linear Accelerator Meeting in Japan*, Sendai, Japan, Aug. 2–4, 2006.
[4] Yokogawa Electric Corporation.
[5] Rika-Lite, NIPPON RIKA KOGYOSHO CO., LTD.